Proceedings of *RAGtime 17–19, 17–19/23–26 Oct., 1–5 Nov., 2015/2016/2017, Opava, Czech Republic*
Z. Stuchlík, G. Török and V. Karas, editors, Silesian University in Opava, 2017, pp. 237–252

Polarization properties of bow shock sources close to the Galactic centre

M. Zajaček[1,2,3,a], V. Karas[3], E. Hosseini[2,1], A. Eckart[2,1], B. Shahzamanian[2], M. Valencia-S.[2], F. Peissker[2], G. Busch[2], S. Britzen[1] and J. A. Zensus[1]

[1] Max-Planck-Institut für Radioastronomie (MPIfR), Auf dem Hügel 69, D-53121 Bonn, Germany
[2] I. Physikalisches Institut der Universität zu Köln, Zülpicher Strasse 77, D-50937 Köln, Germany
[3] Astronomical Institute, Academy of Sciences, Boční II 1401, CZ-14131 Prague, Czech Republic
[a] zajacek@ph1.uni-koeln.de

ABSTRACT
Several bow shock sources were detected and resolved in the innermost parsec from the supermassive black hole in the Galactic centre. They show several distinct characteristics, including an excess towards mid-infrared wavelengths and a significant linear polarization as well as a characteristic prolonged bow-shock shape. These features give hints about the presence of a non-spherical dusty envelope generated by the bow shock. The Dusty S-cluster Object (also denoted as G2) shows similar characteristics and it is a candidate for the closest bow shock with a detected proper motion in the vicinity of Sgr A*, with the pericentre distance of only approx. 2000 Schwarzschild radii. However, in the continuum emission it is a point-like source and hence we use Monte Carlo radiative transfer modeling to reveal its possible three-dimensional structure. Alongside the spectral energy distribution, the detection of polarized continuum emission in the near-infrared K_s-band (2.2 micrometers) puts additional constraints on the geometry of the source.

Keywords: black hole physics – Galaxy: centre – radiative transfer – polarization – stars: pre-main-sequence

1 BOW SHOCKS CLOSE TO THE GALACTIC CENTRE

The Galactic centre region serves as a unique laboratory to study the mutual interaction of stars with the ambient gaseous-dusty medium (Genzel et al., 2010; Mužić et al., 2010). Inside the sphere of gravitational influence of the supermassive black hole (hereafter SMBH) of $M_\bullet \simeq 4 \times 10^6\, M_\odot$ (Parsa et al., 2017), which is associated with the compact radio source

978-80-7510-257-7

Sgr A*, stars exhibit a Keplerian rise (Eckart and Genzel, 1996, 1997) in orbital velocities $v_\star \propto r^{-1/2}$, with the typical Keplerian velocities as large as

$$v_\star \simeq 415 \left(\frac{M_\bullet}{4\times10^6\,M_\odot}\right)^{1/2}\left(\frac{r}{0.1\,\mathrm{pc}}\right)^{-1/2}\ \mathrm{km\,s^{-1}}\ \text{for}\ r \lesssim r_{\mathrm{inf}}, \tag{1}$$

where r is the radial distance from the SMBH. The radius of the gravitational influence of the SMBH represents the length-scale on which the gravitational potential of the SMBH prevails over the potential of the Nuclear Star Cluster, which is proportional to the square of the one-dimensional stellar velocity dispersion $\sigma_\star$ (see e.g. Schneider, 2006; Merritt, 2013; Generozov et al., 2015),

$$r_{\mathrm{inf}} \simeq GM_\bullet/\sigma_\star^2 = 1.7\left(\frac{M_\bullet}{4\times10^6\,M_\odot}\right)\left(\frac{\sigma_\star}{100\,\mathrm{km\,s^{-1}}}\right)^{-2}\ \mathrm{pc}\,. \tag{2}$$

Using the empirical SMBH mass–velocity disperion correlation $M_\bullet - \sigma_\star$ (Ferrarese and Merritt, 2000; McConnell et al., 2011) in the form (McConnell et al., 2011)

$$M_\bullet \simeq 2\times10^8\left(\frac{\sigma_\star}{200\,\mathrm{km\,s^{-1}}}\right)^{5.1}\ M_\odot\,, \tag{3}$$

the influence radius (2) can be expressed as a function of the SMBH mass only,

$$r_{\mathrm{inf}} \simeq 2\left(\frac{M_\bullet}{4\times10^6\,M_\odot}\right)^{0.6}\ \mathrm{pc}\,, \tag{4}$$

which keeps the influence radius at about 2 pc for the Galactic centre region. Inside this radius the inner rim of the atomic and the molecular circum-nuclear ring (CND) is located, which has an inner radius at $\sim$ 1.5 pc (Harada et al., 2015). Further in towards the SMBH, there is a cavity that is filled mostly with rarefied diffuse ionized gas (Becklin et al., 1982; Montero-Castaño et al., 2009). A distinct feature is the minispiral that represents a denser concentration of colder ionized and neutral gas and dust and its dynamics is represented by three bundles of quasi-Keplerian orbits (see Moser et al., 2017and references therein). The rest of the gas is mostly supplied by the winds of massive OB/Wolf-Rayet stars and its dynamics can be approximated by the radial inflow/outflow towards/from the SMBH (Cuadra et al., 2006). The gas supplied by stars is bound to the SMBH inside the Bondi radius r_{B}, inside which the gravitational potential of the SMBH overcomes the pressure of the gas,

$$r_{\mathrm{B}} \simeq \frac{2GM_\bullet}{c_{\mathrm{s}}^2} \approx 0.15\left(\frac{M_\bullet}{4\times10^6\,M_\odot}\right)\left(\frac{\mu_{\mathrm{HII}}}{0.5}\right)\left(\frac{\gamma}{1.4}\right)^{-1}\left(\frac{T_{\mathrm{a}}}{10^7\,\mathrm{K}}\right)^{-1}\ \mathrm{pc}\,, \tag{5}$$

where the mean molecular weight is scaled to $\mu_{\mathrm{HII}} = 0.5$, which corresponds to the fully ionized HII region (Lang, 1978). The temperature of the ambient medium is expressed in 10^7 K, which is based on the thermal bremsstrahlung emission of hot ionized plasma in the central parsec. The fit of the bremsstrahlung emissivity to the observed surface brightness profile yields the electron temperature of $k_{\mathrm{B}}T_{\mathrm{e}} \in [1; 2; 3.5\,\mathrm{keV}]$ ($T_{\mathrm{e}} = 11.6 - 40.6\times10^6$ K)

at the Bondi radius based on different dynamical models – radiatively inefficient accretion flow (RIAF) (Wang et al., 2013), stellar outflows (Shcherbakov and Baganoff, 2010), and the spherical steady Bondi flow (Różańska et al., 2015), respectively. Depending on whether the flow is adiabatic ($\gamma = 5/3$) or isothermal ($\gamma = 1$), the Bondi radius can extend from ~ 0.1 pc up to ~ 0.2 pc within the uncertainties of adopted parameters, respectively. The steady inflow-outflow flow solution in the Galactic centre region is illustrated in Fig. 2. In general the structure of the flow inside the classical Bondi radius is expected to be more complex, possibly non-spherical. This is hinted by the fact that the accretion rate at the Bondi radius is $\dot{M}_{\rm B} = 1 \times 10^{-5}\,{\rm M}_{\odot}\,{\rm yr}^{-1}$ (Baganoff et al., 2003), whereas the SMBH associated with Sgr A* was inferred to accrete at much smaller rate based on the Faraday rotation measurements, $\dot{M}_{\rm SgrA*} = 2\times10^{-9} - 2\times10^{-7}{\rm M}_{\odot}\,{\rm yr}^{-1}$ (Marrone et al., 2007), which implies a significant outflow even inside the Bondi sphere. However, the steady spherical inflow-outflow structure is still a relevant approximation of the Galactic centre processes and we will adopt it further for analytical and semi-analytical estimates of the star–ambient medium interaction.

The radial distance in Eq. (1) is scaled to the length-scale of 0.1 pc, which is within the distance range where ~ 200 young, massive stars of spectral type OB are located (~ 0.04-0.5 pc Buchholz et al., 2009; Bartko et al., 2010). These recently formed luminous stars provide a significant fraction of the kinetic energy and material via their fast outflows and due to their large orbital velocities given by Eq. (1), they are observed to interact with the ambient medium in the form of *bow shocks* (Mužić et al., 2010; Rauch et al., 2013; Sanchez-Bermudez et al., 2014). These are clearly detected as extended non-spherical dusty shells in infrared bands that exhibit a thermal excess towards mid-infrared bands as well as an intrinsic linearly polarized emission (Buchholz et al., 2011, 2013).

The basic condition for the formation of shocks in the interstellar medium (ISM) is that the relative velocity of the source $\mathbf{v}_{\rm rel}$ (star, cloud) with respect to the ambient medium is supersonic. The bow shock that forms is aligned with respect to the relative velocity vector $\mathbf{v}_{\rm rel} = \mathbf{v}_{\star} - \mathbf{v}_{\rm a}$. In case the ionized gas is non-magnetized, the perturbations and signals in the medium move at the sound speed $c_{\rm s}$,

$$c_{\rm s} = 482 \left(\frac{\gamma}{1.4}\right)^{1/2} \left(\frac{T_{\rm a}}{10^7\,{\rm K}}\right)^{1/2} \left(\frac{\mu_{\rm HII}}{0.5}\right)^{-1/2} \ {\rm km\,s^{-1}}, \tag{6}$$

which means that the Mach number $\mathcal{M} \equiv v_{\rm rel}/c_{\rm s}$ at the Bondi radius is close to unity for a non-magnetized medium since the orbital velocity and the sound speed are comparable, see Eqs. (1) and (6).

Based on the multi-frequency observations of the Galactic centre magnetar (Eatough et al., 2013), a large, dynamical important magnetic field intensity was found based on the Faraday rotation measurements, $B \geq 50\,\mu$G on the projected radial scales of $\sim 3'' = 0.12$ pc. Combined with the inferred electron number density of $n_{\rm e}^{\rm out} = 18.3\pm0.1\,{\rm cm}^{-3}$ at the Bondi radius (Różańska et al., 2015), one can estimate the Alfvén velocity that represents the speed at which hydrodynamic waves propagate in the magnetized plasma,

$$v_{\rm A} = \sqrt{\frac{B^2}{\mu_0 \mu m_{\rm H} n_{\rm e}^{\rm out}}} \approx 36 \left(\frac{B}{50\,\mu G}\right) \left(\frac{\mu_{\rm HII}}{0.5}\right)^{-1/2} \left(\frac{n_{\rm e}^{\rm out}}{18.3\,{\rm cm}^{-3}}\right)^{-1/2}, \tag{7}$$

which implies the Alfvénic Mach number $\mathcal{M}_{\rm A} \equiv v_{\rm rel}/v_{\rm A}$ larger than unity and thus supersonic velocities of stars at the Bondi radius in case the plasma is magnetically dominated.

The formation of the shock is given by the interaction between the pressure of the stellar outflow and the ambient ram pressure due to the linear stellar motion. The open bow shock is formed for supersonic relative velocities, when the shock driven into the ambient medium and the shocked stellar wind are separated by the contact discontinuity located at the stand-off distance $R_{\rm bw}$ from the star. However, for fast stellar outflows, the prolonged cavity surrounded by the shocked stellar wind is formed even for subsonic velocities (Christie et al., 2016). In general, it is instructive to look at the distance range in the Galactic centre where the bow shocks can form, which is in general given by the condition $\mathcal{M} \gtrsim 1$ for a non-magnetized plasma or $\mathcal{M}_{\rm A} \gtrsim 1$ for the magnetically dominated environment. For simplicity, we assume that stars move on circular Keplerian orbits and they can interact with stationary medium or inflow/outflow with the ambient velocity $v_{\rm a}^{\rm r} = 1000, 2000,$ and $3000\,{\rm km\,s^{-1}}$. For the ambient medium, we take the radial density and temperature profile as calculated for Bondi spherical flow (Różańska et al., 2015) and RIAF-based flow (Psaltis, 2012). In addition, we consider the profile of the Alfvén velocity calculated according to Eq. (7), where we calculate the magnetic field intensity $B^2 = 8\pi P_{\rm gas}/\beta$, where β is the plasma parameter. We take $\beta = 100$ so that the Alfvén velocity is consistent with the Faraday rotation measurements at the projected distance of $3''$ (Eatough et al., 2013; Różańska et al., 2015).

The occurrence of bow-shock structures in the Galactic centre is expected on a large spatial scale according to Fig. 1 – depending on the ambient temperature profile of the hot diffuse plasma as well as the presence and the velocity of the inflow/outflow, which both affect the Mach number at the given radius $\mathcal{M}(r) = v_{\rm rel}/c_{\rm s}(r)$. The conditions for bow-shock formation inside the sphere of influence are not quite isotropic, mainly because of the presence of the denser and the cooler arms of the Minispiral with the gas temperature in the range of $\sim$ 1000 K–10 000 K (Kunneriath et al., 2012; Moser et al., 2017), which puts the sound speed well below the expected Keplerian velocities of stars. It is thus not a coincidence that several bright bow-shock sources are detected along and close to the Minispiral arms (Wolf-Rayet stars IRS5, IRS1W, IRS10W, IRS21 Sanchez-Bermudez et al., 2014).

2 AMBIENT MEDIUM AND SCALING OF BOW SHOCK SIZES AND LUMINOSITIES

Inside the influence radius, the ambient medium in the Galactic centre is neither stationary nor homogeneous. In fact, it represents a multi-phase medium (Barai et al., 2012; Różańska et al., 2014, 2017) with a complex inflow-outflow structure, see Fig. 2, which is partially represented by radiatively inefficient accretion flows (RIAFs, Yuan and Narayan, 2014) or spherical Bondi solutions (Różańska et al., 2015). In case of a purely hydrodynamical accretion, transonic behaviour is typical for black hole inflows at small radii, where the inward-directed speed of the medium reaches and exceeds the speed of sound (e.g., Chakrabarti, 1990; Das et al., 2015). This is also the case of accretion onto a rotating black hole; unlike the case of accretion onto a non-rotating black hole, in a rapidly rotating case

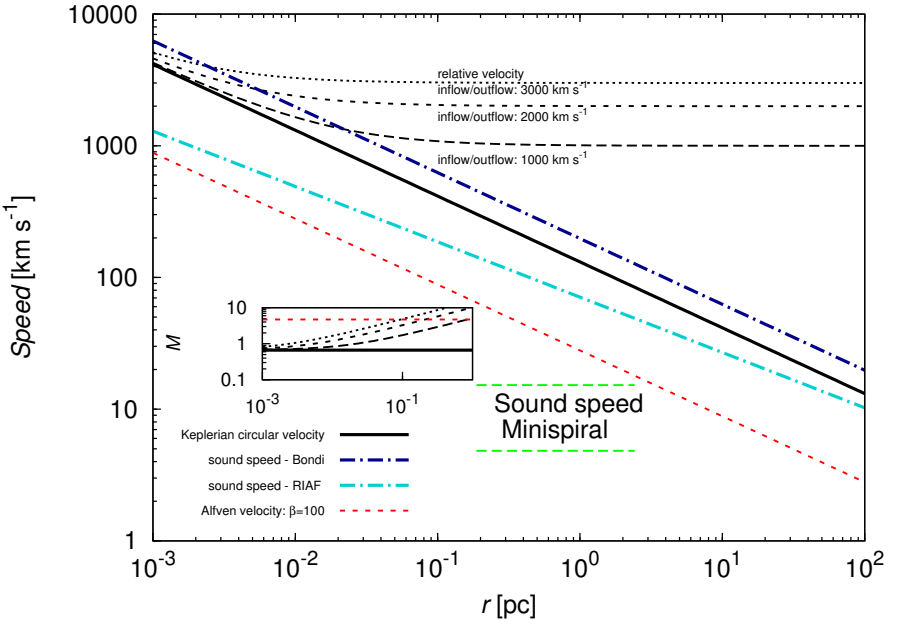

Figure 1. The radial profile of the Keplerian circular velocity, the sound speed for the Bondi flow and RIAF, the relative velocity of the circular stellar motion with respect to the ambient outflow/inflow. There is a lower sound speed in the denser and cooler Minispiral arms, which is shown by green dashed lines. The profile of the Alfvén velocity is also depicted for the plasma parameter $\beta = 100$. The plot inset shows the Mach numbers for the Keplerian circular velocity and corresponding relative velocities with respect to the sound speed and the Alfvén velocity in the Bondi flow (Różańska et al., 2015).

the medium acquires azimuthal velocity in the course of infall (Pariev, 1996). This arises due to the effect of frame dragging, which occurs at small radii just above the black hole ergosphere.

Unlike the classical purely hydrodynamical Bondi spherical accretion, where no additional energy input (heat or mechanical driving by winds) is available, in the case of Sgr A* there are indeed such sources present due to stars of the Nuclear Stellar Cluster (Silich et al., 2008). This can act against the gravitational pull of the central black hole and reverse the direction of the medium inflow in the inner regions to outflow above a transitional, so-called stagnation radius. In consequence, the bow-shock interaction with the ambient medium of changing velocity will affect the orientation and the overall shape of the bow-shock. The motion of the ambient medium can be revealed either by the combination of the stellar proper motion and bow-shock orientation for extended sources or by the detection of polarized emission for unresolved sources.

It is instructive to calculate the change of the bow-shock size as well as the overall thermal luminosity of the bow shock along the orbit. This is possible under the assumption

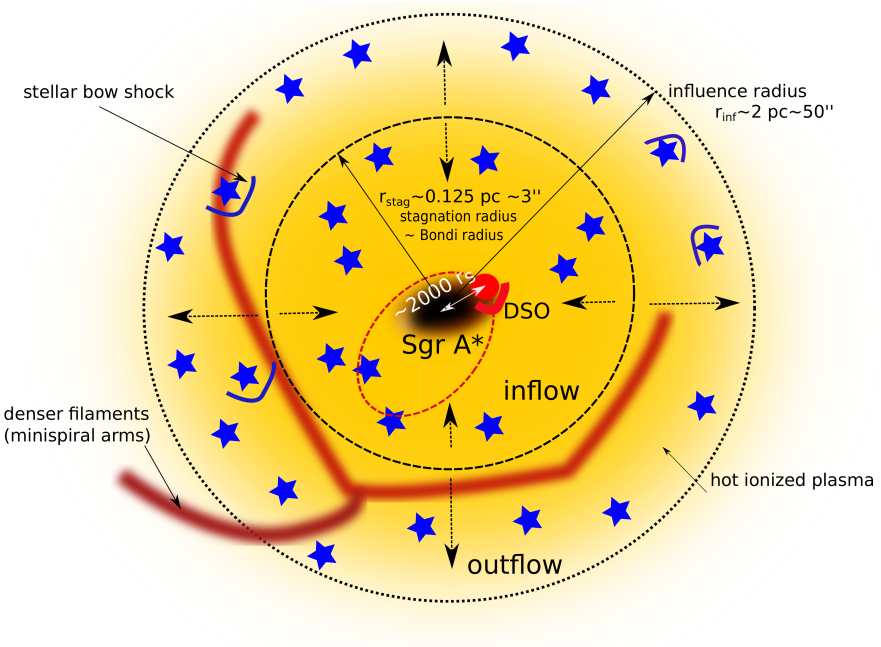

Figure 2. Illustration of the Galactic centre region within the sphere of influence. Two main regions may be distinguished: inside the stagnation radius the inflow of gas takes place, outside it the gas flows out. Stars of the Nuclear Star Cluster are located in both regions. When the relative velocity of the star is larger than the local sound speed, the bow shock forms. Its size and gas and dust density depend on both stellar parameters (the stellar mass-loss rate $\dot{m}_{\rm w}$ and the terminal stellar wind velocity $v_{\rm w}$) and the local ambient density $\rho_{\rm a}$ as well as the relative velocity $v_{\rm rel}$.

of the Keplerian motion around the SMBH (Sgr A*) and the prescription for the radial density profile, $n_{\rm a} = n_{\rm a0}(r/r_0)^{-\nu}$, where $n_{\rm a0}$ is the ambient density at the distance r_0 from the SMBH and ν denotes the index of the power-law ambient density. The relations between two positions along the orbit are especially simple and elegant for an elliptic orbit, which is valid for most of the stars in the innermost S cluster (Zajaček et al., 2016), and under the assumption that $\mathbf{v}_{\rm rel} = \mathbf{v}_\star$, i.e. the motion of the ambient medium is negligible, which is especially the case at and close to the stagnation radius $r_{\rm stag}$, where the radial gas velocity passes through zero.

The relation for the stagnation radius can be found within a one-dimensional steady-state inflow-outflow model of the gas in the vicinity of a galactic nucleus (Generozov et al., 2015). The gas supplied to the interstellar medium by stellar winds flows towards the black hole inside $r_{\rm stag}$ and a fraction of the matter is accreted into the SMBH, while the gas outside $r_{\rm stag}$ forms a radial outflow, see Fig 2. When considering bright massive OB stars in the inner parsec of the Galactic centre (Paumard et al., 2006; Bartko et al., 2010), the heating rate due to their fast outflows $v_{\rm w}$ is typically larger than the stellar velocity dispersion $\sigma_\star$ of the cluster, $v_{\rm w} \gg \sigma_\star$. In this case, the stagnation radius can be approximately expressed

as (Generozov et al., 2015),

$$r_{\rm stag} \approx \left(\frac{13+8\Gamma}{4+2\Gamma} - \frac{3\nu_{\rm stag}}{2+\Gamma}\right)\frac{GM_\bullet}{\nu_{\rm stag} v_{\rm w}^2} \approx \begin{cases} 0.30\left(\frac{M_\bullet}{4\times10^6\,M_\odot}\right)\left(\frac{v_{\rm w}}{500\,{\rm km\,s^{-1}}}\right)^{-2}\,{\rm pc} & ,{\rm core}\ (\Gamma=0.1)\,, \\ 0.16\left(\frac{M_\bullet}{4\times10^6\,M_\odot}\right)\left(\frac{v_{\rm w}}{500\,{\rm km\,s^{-1}}}\right)^{-2}\,{\rm pc} & ,{\rm cusp}\ (\Gamma=0.8)\,, \end{cases} \tag{8}$$

where Γ is the power-law index of the inner stellar brightness profile. For estimative purposes, we consider two limiting cases, the core profile with $\Gamma = 0.1$ and the stellar cusp with $\Gamma = 0.8$. The quantity $\nu_{\rm stag} = -{\rm d}n_{\rm a}/{\rm d}r|_{r_{\rm stag}}$ is the gas density power-law slope at $r_{\rm stag}$, which according to the numerical analysis of Generozov et al. (2015) is $\nu_{\rm stag} \approx 1/6[(4\Gamma+3)]$. According to the estimates in Eq. (8), the stagnation radius is expected to be located close to the Bondi radius with an offset given by the numerical factor (Generozov et al., 2015)

$$\frac{r_{\rm stag}}{r_{\rm B}} \approx \frac{13+8\Gamma}{(2+\Gamma)(3+4\Gamma)}\,, \tag{9}$$

which is of the order of unity. This is also illustrated in the two-zone scheme in Fig. 2.

Under the assumption that the stellar-wind pressure is at the equilibrium with the ram pressure and the thermal pressure of the medium $P_{\rm w} = P_{\rm ram} + P_{\rm th} = P_{\rm ram}(1+\alpha)$, where $\alpha = P_{\rm th}/P_{\rm ram}$, one can express the characteristic length-scale – or stand-off distance R_0 – using the following generalized formula (Wilkin, 1996; Zhang and Zheng, 1997; Christie et al., 2016),

$$R_0 = \left(\frac{\dot{m}_{\rm w} v_{\rm w}}{\Omega_{\rm w}\rho_{\rm a} v_{\rm rel}^2(1+\alpha)}\right)^{1/2} \simeq C_\star \rho_{\rm a}^{-1/2} v_{\rm rel}^{-1}\,, \tag{10}$$

where $\dot{m}_{\rm w}$ is the stellar mass-loss rate, $v_{\rm w}$ is the terminal wind velocity, and $\Omega_{\rm w}$ is the solid angle into which the stellar wind is blown (for the isotropic case that is often assumed, $\Omega_{\rm w} = 4\pi$). The last equality in Eq. 10 is valid in case the ratio of the thermal pressure to the ram pressure α is negligible, which is for highly supersonic motion, $\mathcal{M} = v_{\rm rel}/c_{\rm s} = 1/\sqrt{\gamma\alpha} \gg 1$ when $\alpha \to 0$. The quantity $C_\star^2 = \dot{m}_{\rm w} v_{\rm w}/\Omega_{\rm w}$ is the momentum flux of the stellar wind per unit solid angle. It can be assumed to be constant per several orbital periods of a star around the SMBH. For the brightest star in the S-cluster S2 star (Martins et al., 2008), the momentum flux can be evaluated as

$$C_\star^2 = 7.85\times10^{-5}\left(\frac{\dot{m}_{\rm w}}{10^{-7}\,M_\odot\,{\rm yr^{-1}}}\right)\left(\frac{v_{\rm w}}{1000\,{\rm km\,s^{-1}}}\right) M_\odot\,{\rm km\,s^{-1}\,yr^{-1}\,sr^{-1}}\,. \tag{11}$$

Under the assumption that the motion of ambient medium is negligible, we can relate the relative velocity to the orbital velocity of the star $v_{\rm rel} \simeq v_\star = \sqrt{GM_\bullet(2/r - 1/a)}$, where we assumed the Keplerian motion of a star around the SMBH with semi-major axis a and we applied the *vis-viva* equation. When we neglect the thermal pressure, we can relate the bow-shock length-scales R_{01} and R_{02} between two respective positions r_1 and r_2 ($r_1 > r_2$) as follows,

$$\frac{R_{01}(r_1)}{R_{02}(r_2)} = \left(\frac{n_{\rm a2}}{n_{\rm a1}}\right)^{1/2}\left(\frac{v_{\rm rel2}}{v_{\rm rel1}}\right) = \left(\frac{r_1}{r_2}\right)^{\nu/2}\left(\frac{v_{\star2}}{v_{\star1}}\right). \tag{12}$$

Using the *vis-viva* integral, we can express the ratio in Eq. (12) as a function of four variables,

$$\frac{R_{01}}{R_{02}}(r_1, r_2, a, \nu) = \left(\frac{r_1}{r_2}\right)^{(\nu+1)/2} \left(\frac{2a - r_2}{2a - r_1}\right)^{1/2} . \tag{13}$$

Even simpler relations can be obtained when evaluating the ratio in Eq. (13) at special points along the elliptical orbit, e.g. between the apobothron and the peribothron of a star orbiting the SMBH,

$$\frac{R_{\rm A}}{R_{\rm P}}(e, \nu) = \left(\frac{1+e}{1-e}\right)^{\frac{\nu}{2}+1} , \tag{14}$$

or between semi-latus rectum (the true anomaly of 90°) and the peribothron,

$$\frac{R_{90}}{R_{\rm P}}(e, \nu) = \frac{(1+e)^{\nu/2+1}}{(1+e^2)^{1/2}} . \tag{15}$$

Since the star on a bound elliptical orbit around the SMBH changes its relative velocity (because of both the change in the orbital velocity and the ambient flow velocity), the bow-shock luminosity is also expected to change. The upper limit for the thermal bow-shock luminosity $L_{\rm th}$ can be obtained from the sum of the kinetic terms of the flow that are assumed to become fully thermalized (Wilkin et al., 1997),

$$L_{\rm th} = \frac{1}{2}\dot{m}_{\rm w}(v_{\rm rel}^2 + v_{\rm w}^2) \simeq \frac{1}{2}\dot{m}_{\rm w}(v_\star^2 + v_{\rm w}^2) . \tag{16}$$

The ratio of the bow-shock luminosities at two different radii along the elliptical orbit may be then simply calculated according to,

$$\frac{L_{\rm th1}}{L_{\rm th2}} = \frac{\beta_1^2 + 1}{\beta_2^2 + 1} , \tag{17}$$

where $\beta = v_{\rm rel}/v_{\rm w} \simeq v_\star/v_{\rm w}$.

In Table 1, we calculate both the ratio of bow-shock sizes according to Eq. (14) and luminosities according to Eq. (17) between the apocentre and the pericentre for different values of the density power-law index ν as well as different orbital eccentricities e. As a prototype of B-type stars in the innermost arcsecond in the S cluster, we take the brightest S2 star with $a \simeq 0.126''$, $e \simeq 0.884$, $\dot{m}_{\rm w} \simeq 10^{-7}\, M_\odot {\rm yr}^{-1}$, and $v_{\rm w} \simeq 1000\,{\rm km\,s}^{-1}$ (Martins et al., 2008; Parsa et al., 2017).

3 MODELLING POLARIZED BOW-SHOCK EMISSION: DUSTY S-CLUSTER OBJECT (DSO/G2) AS A SPECIAL CASE OF UNRESOLVED BOW SHOCK CLOSE TO THE BLACK HOLE

Of special interest is a stellar bow shock located in the direct vicinity of the SMBH. The Galactic centre is the only nucleus where we can study the individual proper motion of

e	ν	R_A/R_P	L^A_{th}/L^P_{th} (S2 star)
0.0	≥ 0	1.0	1.0
0.50	0.0	3.00	0.19
0.50	0.5	3.95	0.19
0.50	1.0	5.20	0.19
0.50	2.0	9.00	0.19
0.90	0.0	19.00	1.8×10^{-2}
0.90	0.5	39.67	1.8×10^{-2}
0.90	1.0	82.82	1.8×10^{-2}
0.90	2.0	361.00	1.8×10^{-2}
0.95	0.0	39.00	8.1×10^{-3}
0.95	0.5	97.46	8.1×10^{-3}
0.95	1.0	243.55	8.1×10^{-3}
0.95	2.0	1521.00	8.1×10^{-3}

Table 1. The ratio of bow-shock sizes R_A/R_P as well as the ratio of thermal bow-shock luminosities L^A_{th}/L^P_{th} between the apocentre and the pericentre of the orbit for different orbital eccentricities and the power-law indices of the gas density profile. We adopted the parameters of S2 star, $a \simeq 0.126''$, $e \simeq 0.884$, $\dot{m}_w \simeq 10^{-7}\, M_\odot \mathrm{yr}^{-1}$, and $v_w \simeq 1000\,\mathrm{km\,s}^{-1}$ (Martins et al., 2008; Parsa et al., 2017), for the calculation of the ratio of bow-shock luminosities.

stars as well as study the interaction of stars with their environment. Although currently there is no bow shock detected on the scale of $\sim$ 10–100 Schwarzschild radii, on which some of the strong-gravity effects could be studied (Dovčiak et al., 2004), Dusty S-cluster Object (DSO/G2; Gillessen et al., 2012; Eckart et al., 2013; Phifer et al., 2013; Witzel et al., 2014; Valencia-S. et al., 2015) shows several signs of an unresolved bow-shock source with the closest distance to the SMBH at $\sim$ 2000 Schwarzschild radii. The main properties of DSO/G2 are the following,

- observed as a bright L'-band (3.8 μm) source. The fitted single-temperature black-body yields the radius of the optically thick photosphere of $R_{DSO} = (0.31 \pm 0.07)$ AU and the temperature of $T_{DSO} = (874 \pm 54)$ K (Zajaček et al., 2017),
- clear infrared-excess (in comparison with main-sequence stars; Eckart et al., 2013; Shahzamanian et al., 2016; Zajaček et al., 2017), which implies the presence of dust,
- a strong emission line of Brγ (but also HeI and Paα), which implies the presence of either inflow or outflow to/from the star (Valencia-S. et al., 2015),
- a significant linearly polarized continuum emission in K_s-band (2.2 μm) with the polarization degree of $p_L = (30 \pm 15)\%$ and a variable polarization angle (Shahzamanian et al., 2016). In continuum, the source is point-like (Witzel et al., 2014; Shahzamanian et al., 2016), and hence the overall non-zero polarization implies a non-spherical nature.

In order to set-up a three-dimensional model of the Dusty S-cluster Object (DSO) – a star with non-spherical dusty envelope – in terms of the continuum emission, we used the Monte Carlo Radiative Transfer code (MCRT) `Hyperion` (Robitaille, 2011). The MCRT

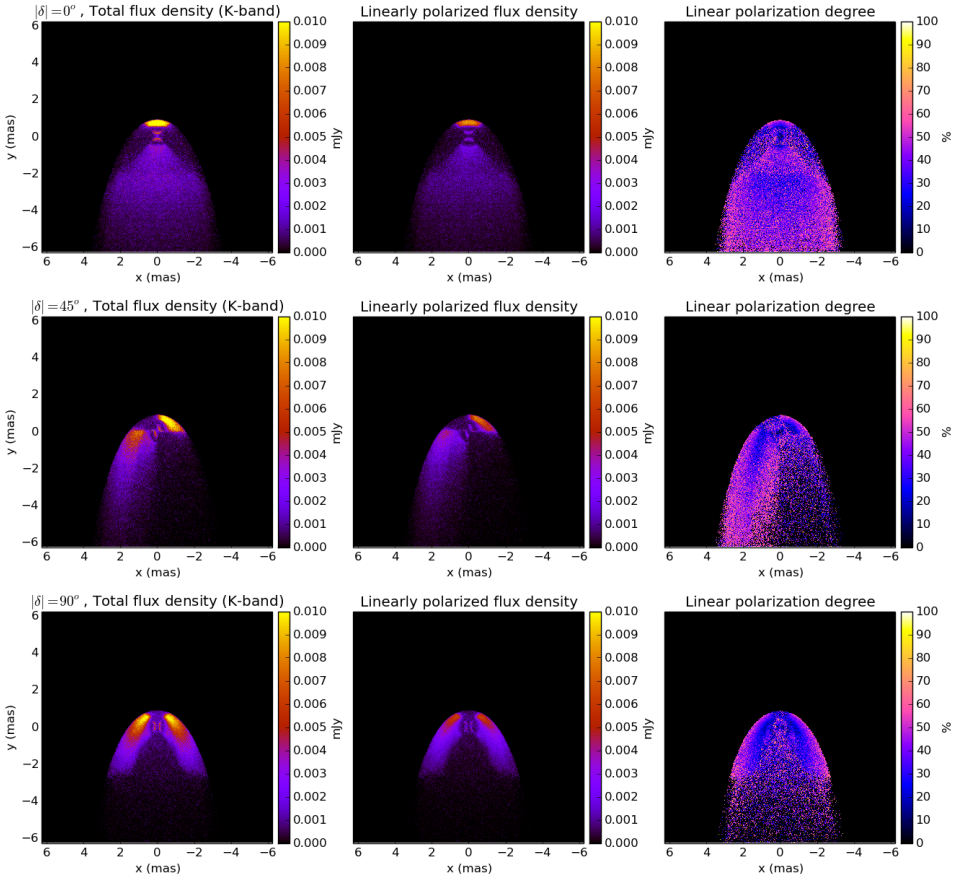

Figure 3. Individual rows represent simulated images of the Dusty S-cluster Object (DSO/G2) for different position angles of the bipolar outflow with respect to the bow-shock symmetry axis: $\delta = 0°$ – top row (the bow shock and the bipolar outflow are aligned), $\delta = 45°$ – middle row, and $\delta = 90°$ – bottom row. In the left column, figures show simulated images in K_s-band (2.2 μm), figures in the middle panel show linearly polarized continuum emission in the same band, and in the right column, images show the maps of the polarization degree.

mimics real observations in a sense that it allows to track photons from their emission by a source, through their propagation through a density field in the medium, until they reach the observer. For the fundamental theory of radiative transfer, first one needs to define the specific intensity I_ν of a beam of light that passes through surface area of dA at an angle of θ to the surface normal within a solid angle dΩ in a time interval dt and a frequency range of dν,

$$I_\nu = \frac{\mathrm{d}E_\nu}{\mathrm{d}A\cos\theta\mathrm{d}\nu\mathrm{d}\Omega\mathrm{d}t}\,. \tag{18}$$

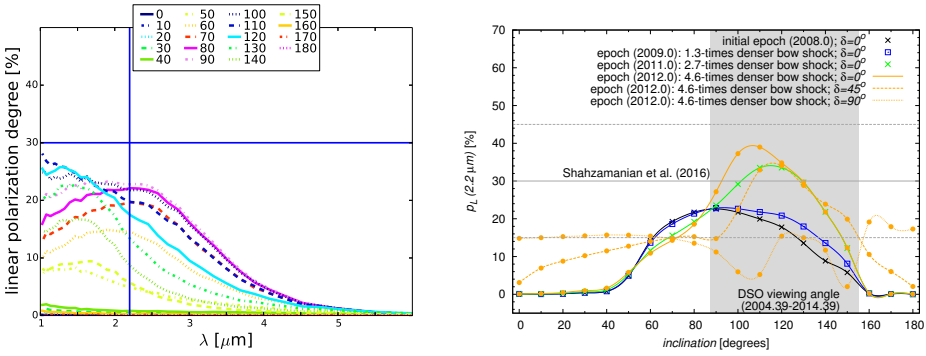

Figure 4. Left panel: The dependency of the linear polarization degree $p_{\rm L}$ $K_{\rm s}$-band (2.2 μm) on the wavelength λ expressed in μm. Different lines correspond to different viewing angles with respect to the observer (0° represents the front view of the bow shock, 90° the side view, and 180° the tail view of the bow shock). The vertical line represents the wavelength of 2.2 μm and the horizontal line stands for the polarization degree of 30%. **Right panel:** The dependency of the linear polarization degree $p_{\rm L}$ in $K_{\rm s}$-band (2.2 μm) on the viewing angle (using the same definition as in the left panel). Different lines correspond to different bow-shock densities as the DSO approached Sgr A* (according to the legend). In addition, for one epoch we also plot the dependencies for different position angles of the bipolar outflow with respect to the bow shock. The dark-gray dashed horizontal lines mark the polarization degree of $p_{\rm L} \simeq (30 \pm 15)\%$ as inferred by Shahzamanian et al. (2016).

The change of the specific intensity through the medium segment dl is governed by the equation of the radiative transfer,

$$\frac{{\rm d}I_\nu}{{\rm d}l} = -\kappa_\nu \rho I_\nu + j_\nu \rho \,, \tag{19}$$

where κ_ν is the opacity of the medium and j_ν is the emissivity, which are both complex functions of the composition and dynamics of the medium as well as of the radiation frequency ν. Eq. (19) can be rewritten in terms of the optical depth τ_ν along the line of sight L,

$$\tau_\nu = -\int_0^L \kappa_\nu \rho {\rm d}l \,, \tag{20}$$

into the form

$$\frac{{\rm d}I_\nu}{{\rm d}\tau_\nu} = I_\nu - S_\nu \,, \tag{21}$$

where $S_\nu = j_\nu/\kappa_\nu$ is the source function of the medium. The transfer equation can be analytically solved only for a certain set of simple problems, e.g. homogeneous plan-parallel layers or isotropic spherical problems. For more complicated cases, it must be solved numerically. In case of three-dimensional dusty stellar atmospheres and envelopes, the MCRT method is currently applied as it can handle the calculation of both total as well as polarized continuum spectral energy distributions and images (Robitaille, 2011).

When a photon interacts with the gaseous-dusty medium, it can either be scattered or absorbed (and emitted in other direction and different wavelength). The scattering probability is given by the *albedo function a*, which can be expressed as follows,

$$a = \frac{n_{\rm s}\sigma_{\rm s}}{n_{\rm s}\sigma_{\rm s} + n_{\rm a}\sigma_{\rm a}}\,, \tag{22}$$

where $n_{\rm s}$ and $n_{\rm a}$ are number densities of scatterers and absorbers, respectively, and $\sigma_{\rm s}$ and $\sigma_{\rm a}$ are cross-sections for scattering and absorbing, respectively.

The scattering of a photon, e.g. by a dust particle, is described by the angular phase function $P(\cos\theta)$. For an isotropic scattering, we have $P(\cos\theta) = 1/2$ and for Rayleigh scattering $P(\cos\theta) = 3/8(1 + \cos^2\theta)$.

The probability that a photon interacts on the length-scale x is given by

$$P(\tau) = 1 - \exp(-\tau)\,, \tag{23}$$

where $\tau = -\int_0^x \kappa\rho {\rm d}x'$. The MCRT then proceeds in three basic steps:

(1) The emission of N photon packets that further propagate through the medium.

(2) The site of the interaction of the photon packet in the medium is found by sampling the optical depth τ_ν from the probability distribution given by Eq. (23). The character of interaction (scattering or absorption) is determined by sampling from albedo and angular phase functions, Eq. (22).

(3) Photons that escape the medium (are not absorbed, but can be scattered) are counted on an image plane (mimicking CCD detectors for real observations) or are binned in frequency intervals for calculating spectral energy distributions.

The advantage of the MCRT is that it describes individual photon packets with the full Stokes vector $\mathbf{S} = (I, Q, U, V)$, which allows us to easily construct polarization maps of the source as well as to calculate the total polarization degree as well as the angle. It was thus possible to compare the radiative properties of the DSO model with the observational analysis of Shahzamanian et al. (2016), who detected a significant polarized emission in the NIR $K_{\rm s}$ for the DSO. The model of the DSO included a young stellar object of class I that is still embedded in the optically thick dusty envelope within its tidal Hill radius. The source exhibits a relatively large polarization degree of $p_{\rm L} \sim 30\%$, which is most probably caused by the presence of bipolar outflows as well as a bow-shock dusty layer. These components significantly break the spherical symmetry (see Zajaček et al., 2017 for a detailed analysis and discussion). In Fig. 3, we show the simulated images of the DSO model, in which one can clearly see the bow-shock layer. From the left to the right panels, images of the continuum, polarized emission as well as the polarization degree in $K_{\rm s}$-band, respectively, are presented. In the left panel of Fig. 4, the polarization degree as a function of wavelength is depicted for different viewing angles. The polarization degree as a function of the viewing angle is specifically shown in the right panel of Fig. 4, where the shaded area is the viewing angle for the years when the DSO was intensively monitored. In our model, we can obtain the polarization degree as large as $\sim 30\%$ depending on the density of the bow shock, which is expected to increase as the DSO approaches the SMBH.

4 CONCLUSIONS

We presented an introductory analysis of the inflow-outflow structure of the Galactic centre environment in the sphere of gravitational influence of the SMBH. The focus was put on the analysis of conditions under which stellar bow shocks can develop. We found that these structures are expected to be present across the broad spatial scale of the Nuclear Star Cluster, which is further supported by the detection and analysis of several bright bow-shock sources in the NIR and MIR-bands. In addition, we derived useful formulae for the scaling of bow-shock sizes as well as thermal luminosities in the vicinity of the SMBH.

In the end, we presented the theoretical basics for Monte Carlo modelling of radiative properties of bow-shock sources and non-spherical circumstellar envelopes in general. We applied the MCRT to the case of the NIR-excess source DSO. The comparison of observations with the MCRT model allows us to draw the conclusion that the NIR continuum characteristics of the DSO are consistent with a young stellar object of class I surrounded by an optically thick dusty envelope dissected by bipolar cavities. Since the DSO is expected to move mildly supersonically close to its peribothron, it should develop a bow shock whose properties can vary along the orbit, depending on the relative velocity of the source as well as the density gradient of the ambient medium.

ACKNOWLEDGEMENTS

We received funding from the European Union Seventh Framework Program (FP7/2013 – 2017) under grant agreement no 312789 - Strong gravity: Probing Strong Gravity by Black Holes Across the Range of Masses. This work was supported in part by the Deutsche Forschungsgemeinschaft (DFG) via the Cologne Bonn Graduate School (BCGS), the Max Planck Society through the International Max Planck Research School (IMPRS) for Astronomy and Astrophysics, as well as special funds through the University of Cologne and SFB 956 Conditions and Impact of Star Formation. M. Zajaček and E. Hosseini are members of the International Max Planck Research School at the Universities of Cologne and Bonn. The authors thank the Czech Ministry of Education Youth and Sports project INTER-INFORM, ref. LTI17018, in cooperation with Silesian University in Opava.

REFERENCES

Baganoff, F. K., Maeda, Y., Morris, M., Bautz, M. W., Brandt, W. N., Cui, W., Doty, J. P., Feigelson, E. D., Garmire, G. P., Pravdo, S. H., Ricker, G. R. and Townsley, L. K. (2003), Chandra X-Ray Spectroscopic Imaging of Sagittarius A* and the Central Parsec of the Galaxy, *ApJ*, **591**, pp. 891–915, arXiv: arXiv:astro-ph/0102151.

Barai, P., Proga, D. and Nagamine, K. (2012), Multiphase, non-spherical gas accretion on to a black hole, *MNRAS*, **424**, pp. 728–746, arXiv: 1112.5483.

Bartko, H., Martins, F., Trippe, S., Fritz, T. K., Genzel, R., Ott, T., Eisenhauer, F., Gillessen, S., Paumard, T., Alexander, T., Dodds-Eden, K., Gerhard, O., Levin, Y., Mascetti, L., Nayakshin, S., Perets, H. B., Perrin, G., Pfuhl, O., Reid, M. J., Rouan, D., Zilka, M. and Sternberg, A. (2010), An Extremely Top-Heavy Initial Mass Function in the Galactic Center Stellar Disks, *ApJ*, **708**, pp. 834–840, arXiv: 0908.2177.

Becklin, E. E., Gatley, I. and Werner, M. W. (1982), Far-infrared observations of Sagittarius A - The luminosity and dust density in the central parsec of the Galaxy, *ApJ*, **258**, pp. 135–142.

Buchholz, R. M., Schödel, R. and Eckart, A. (2009), Composition of the galactic center star cluster. Population analysis from adaptive optics narrow band spectral energy distributions, *A&A*, **499**, pp. 483–501, arXiv: 0903.2135.

Buchholz, R. M., Witzel, G., Schödel, R. and Eckart, A. (2013), Ks- and Lp-band polarimetry on stellar and bow-shock sources in the Galactic center, *A&A*, **557**, A82, arXiv: 1308.0956.

Buchholz, R. M., Witzel, G., Schödel, R., Eckart, A., Bremer, M. and Mužić, K. (2011), Adaptive-optics assisted near-infrared polarization measurements of sources in the Galactic center, *A&A*, **534**, A117, arXiv: 1107.3781.

Chakrabarti, S. K. (1990), *Theory of Transonic Astrophysical Flows*, World Scientific Publishing Co.

Christie, I. M., Petropoulou, M., Mimica, P. and Giannios, D. (2016), Modelling accretion disc and stellar wind interactions: the case of Sgr A*, *MNRAS*, **459**, pp. 2420–2431, arXiv: 1601.07432.

Cuadra, J., Nayakshin, S., Springel, V. and Di Matteo, T. (2006), Galactic Centre stellar winds and Sgr A* accretion, *MNRAS*, **366**, pp. 358–372, arXiv: astro-ph/0505382.

Das, T. K., Nag, S., Hegde, S., Bhattacharya, S., Maity, I., Czerny, B., Barai, P., Wiita, P. J., Karas, V. and Naskar, T. (2015), Black hole spin dependence of general relativistic multi-transonic accretion close to the horizon, *NewA*, **37**, pp. 81–104, arXiv: 1211.6952.

Dovčiak, M., Karas, V. and Yaqoob, T. (2004), An Extended Scheme for Fitting X-Ray Data with Accretion Disk Spectra in the Strong Gravity Regime, *ApJS*, **153**, pp. 205–221, arXiv: astro-ph/0403541.

Eatough, R. P., Falcke, H., Karuppusamy, R., Lee, K. J., Champion, D. J., Keane, E. F., Desvignes, G., Schnitzeler, D. H. F. M., Spitler, L. G., Kramer, M., Klein, B., Bassa, C., Bower, G. C., Brunthaler, A., Cognard, I., Deller, A. T., Demorest, P. B., Freire, P. C. C., Kraus, A., Lyne, A. G., Noutsos, A., Stappers, B. and Wex, N. (2013), A strong magnetic field around the supermassive black hole at the centre of the Galaxy, *Nature*, **501**, pp. 391–394, arXiv: 1308.3147.

Eckart, A. and Genzel, R. (1996), Observations of stellar proper motions near the Galactic Centre, *Nature*, **383**, pp. 415–417.

Eckart, A. and Genzel, R. (1997), Stellar proper motions in the central 0.1 PC of the Galaxy, *MNRAS*, **284**, pp. 576–598.

Eckart, A., Mužić, K., Yazici, S., Sabha, N., Shahzamanian, B., Witzel, G., Moser, L., Garcia-Marin, M., Valencia-S., M., Jalali, B., Bremer, M., Straubmeier, C., Rauch, C., Buchholz, R., Kunneriath, D. and Moultaka, J. (2013), Near-infrared proper motions and spectroscopy of infrared excess sources at the Galactic center, *A&A*, **551**, A18, arXiv: 1208.1907.

Ferrarese, L. and Merritt, D. (2000), A Fundamental Relation between Supermassive Black Holes and Their Host Galaxies, *ApJL*, **539**, pp. L9–L12, arXiv: astro-ph/0006053.

Generozov, A., Stone, N. C. and Metzger, B. D. (2015), Circumnuclear media of quiescent supermassive black holes, *MNRAS*, **453**, pp. 775–796, arXiv: 1505.00268.

Genzel, R., Eisenhauer, F. and Gillessen, S. (2010), The Galactic Center massive black hole and nuclear star cluster, *Reviews of Modern Physics*, **82**, pp. 3121–3195, arXiv: 1006.0064.

Gillessen, S., Genzel, R., Fritz, T. K., Quataert, E., Alig, C., Burkert, A., Cuadra, J., Eisenhauer, F., Pfuhl, O., Dodds-Eden, K., Gammie, C. F. and Ott, T. (2012), A gas cloud on its way towards the supermassive black hole at the Galactic Centre, *Nature*, **481**, pp. 51–54, arXiv: 1112.3264.

Harada, N., Riquelme, D., Viti, S., Jiménez-Serra, I., Requena-Torres, M. A., Menten, K. M., Martín, S., Aladro, R., Martin-Pintado, J. and Hochgürtel, S. (2015), Chemical features in the circumnuclear disk of the Galactic center, *A&A*, **584**, A102, arXiv: 1510.02904.

Kunneriath, D., Eckart, A., Vogel, S. N., Teuben, P., Mužić, K., Schödel, R., García-Marín, M.,

Moultaka, J., Staguhn, J., Straubmeier, C., Zensus, J. A., Valencia-S., M. and Karas, V. (2012), The Galactic centre mini-spiral in the mm-regime, *A&A*, **538**, A127, arXiv: 1201.2362.

Lang, K. R. (1978), *Astrophysical formulae. A compendium for the physicist and astrophysicist (Berlin: Springer)*.

Marrone, D. P., Moran, J. M., Zhao, J.-H. and Rao, R. (2007), An Unambiguous Detection of Faraday Rotation in Sagittarius A*, *ApJL*, **654**, pp. L57–L60, arXiv: astro-ph/0611791.

Martins, F., Gillessen, S., Eisenhauer, F., Genzel, R., Ott, T. and Trippe, S. (2008), On the Nature of the Fast-Moving Star S2 in the Galactic Center, *ApJL*, **672**, pp. L119–L122, arXiv: 0711.3344.

McConnell, N. J., Ma, C.-P., Gebhardt, K., Wright, S. A., Murphy, J. D., Lauer, T. R., Graham, J. R. and Richstone, D. O. (2011), Two ten-billion-solar-mass black holes at the centres of giant elliptical galaxies, *Nature*, **480**, pp. 215–218, arXiv: 1112.1078.

Merritt, D. (2013), *Dynamics and Evolution of Galactic Nuclei (Princeton: Princeton University Press)*.

Montero-Castaño, M., Herrnstein, R. M. and Ho, P. T. P. (2009), Gas Infall Toward Sgr A* from the Clumpy Circumnuclear Disk, *ApJ*, **695**, pp. 1477–1494, arXiv: 0903.0886.

Moser, L., Sánchez-Monge, Á., Eckart, A., Requena-Torres, M. A., García-Marin, M., Kunneriath, D., Zensus, A., Britzen, S., Sabha, N., Shahzamanian, B., Borkar, A. and Fischer, S. (2017), Approaching hell's kitchen: Molecular daredevil clouds in the vicinity of Sagittarius A*, *A&A*, **603**, A68, arXiv: 1603.00801.

Mužić, K., Eckart, A., Schödel, R., Buchholz, R., Zamaninasab, M. and Witzel, G. (2010), Comet-shaped sources at the Galactic center. Evidence of a wind from the central 0.2 pc, *A&A*, **521**, A13, arXiv: 1006.0909.

Pariev, V. I. (1996), Hydrodynamic accretion on to a rapidly rotating Kerr black hole, *MNRAS*, **283**, pp. 1264–1280, arXiv: astro-ph/9510008.

Parsa, M., Eckart, A., Shahzamanian, B., Karas, V., Zajaček, M., Zensus, J. A. and Straubmeier, C. (2017), Investigating the Relativistic Motion of the Stars Near the Supermassive Black Hole in the Galactic Center, *ApJ*, **845**, 22, arXiv: 1708.03507.

Paumard, T., Genzel, R., Martins, F., Nayakshin, S., Beloborodov, A. M., Levin, Y., Trippe, S., Eisenhauer, F., Ott, T., Gillessen, S., Abuter, R., Cuadra, J., Alexander, T. and Sternberg, A. (2006), The Two Young Star Disks in the Central Parsec of the Galaxy: Properties, Dynamics, and Formation, *ApJ*, **643**, pp. 1011–1035, arXiv: arXiv:astro-ph/0601268.

Phifer, K., Do, T., Meyer, L., Ghez, A. M., Witzel, G., Yelda, S., Boehle, A., Lu, J. R., Morris, M. R., Becklin, E. E. and Matthews, K. (2013), Keck Observations of the Galactic Center Source G2: Gas Cloud or Star?, *ApJL*, **773**, L13, arXiv: 1304.5280.

Psaltis, D. (2012), The Influence of Gas Dynamics on Measuring the Properties of the Black Hole in the Center of the Milky Way with Stellar Orbits and Pulsars, *ApJ*, **759**, 130, arXiv: 1112.0026.

Rauch, C., Mužić, K., Eckart, A., Buchholz, R. M., García-Marín, M., Sabha, N., Straubmeier, C., Valencia-S., M. and Yazici, S. (2013), A peek behind the dusty curtain: K_S-band polarization photometry and bow shock models of the Galactic center source IRS 8, *A&A*, **551**, A35.

Robitaille, T. P. (2011), HYPERION: an open-source parallelized three-dimensional dust continuum radiative transfer code, *A&A*, **536**, A79, arXiv: 1112.1071.

Różańska, A., Czerny, B., Kunneriath, D., Adhikari, T. P., Karas, V. and Mościbrodzka, M. (2014), Conditions for thermal instability in the Galactic Centre mini-spiral region, *MNRAS*, **445**, pp. 4385–4394, arXiv: 1410.0397.

Różańska, A., Kunneriath, D., Czerny, B., Adhikari, T. P. and Karas, V. (2017), Multiphase environment of compact galactic nuclei: the role of the nuclear star cluster, *MNRAS*, **464**, pp. 2090–2102, arXiv: 1609.08834.

Różańska, A., Mróz, P., Mościbrodzka, M., Sobolewska, M. and Adhikari, T. P. (2015), X-ray observations of the hot phase in Sagittarius A*, *A&A*, **581**, A64, arXiv: 1507.01798.

Sanchez-Bermudez, J., Schödel, R., Alberdi, A., Muzić, K., Hummel, C. A. and Pott, J.-U. (2014), Properties of bow-shock sources at the Galactic center, *A&A*, **567**, A21, arXiv: 1405.4528.

Schneider, P. (2006), *Extragalactic Astronomy and Cosmology (Berlin: Springer)*.

Shahzamanian, B., Eckart, A., Zajaček, M., Valencia-S., M., Sabha, N., Moser, L., Parsa, M., Peissker, F. and Straubmeier, C. (2016), Polarized near-infrared light of the Dusty S-cluster Object (DSO/G2) at the Galactic center, *A&A*, **593**, A131, arXiv: 1607.04568.

Shcherbakov, R. V. and Baganoff, F. K. (2010), Inflow-Outflow Model with Conduction and Self-consistent Feeding for Sgr A*, *ApJ*, **716**, pp. 504–509, arXiv: 1004.0702.

Silich, S., Tenorio-Tagle, G. and Hueyotl-Zahuantitla, F. (2008), Spherically Symmetric Accretion onto a Black Hole at the Center of a Young Stellar Cluster, *ApJ*, **686**, 172-180, arXiv: 0806.3054.

Valencia-S., M., Eckart, A., Zajaček, M., Peissker, F., Parsa, M., Grosso, N., Mossoux, E., Porquet, D., Jalali, B., Karas, V., Yazici, S., Shahzamanian, B., Sabha, N., Saalfeld, R., Smajic, S., Grellmann, R., Moser, L., Horrobin, M., Borkar, A., García-Marín, M., Dovčiak, M., Kunneriath, D., Karssen, G. D., Bursa, M., Straubmeier, C. and Bushouse, H. (2015), Monitoring the Dusty S-cluster Object (DSO/G2) on its Orbit toward the Galactic Center Black Hole, *ApJ*, **800**, 125, arXiv: 1410.8731.

Wang, Q. D., Nowak, M. A., Markoff, S. B., Baganoff, F. K., Nayakshin, S., Yuan, F., Cuadra, J., Davis, J., Dexter, J., Fabian, A. C., Grosso, N., Haggard, D., Houck, J., Ji, L., Li, Z., Neilsen, J., Porquet, D., Ripple, F. and Shcherbakov, R. V. (2013), Dissecting X-ray-Emitting Gas Around the Center of Our Galaxy, *Science*, **341**, pp. 981–983, arXiv: 1307.5845.

Wilkin, F. P. (1996), Exact Analytic Solutions for Stellar Wind Bow Shocks, *ApJL*, **459**, p. L31.

Wilkin, F. P., Canto, J. and Raga, A. C. (1997), On the Energetics and Momentum Distribution of Bow Shocks and Colliding Winds, in B. Reipurth and C. Bertout, editors, *Herbig-Haro Flows and the Birth of Stars*, volume 182 of *IAU Symposium*, pp. 343–352.

Witzel, G., Ghez, A. M., Morris, M. R., Sitarski, B. N., Boehle, A., Naoz, S., Campbell, R., Becklin, E. E., Canalizo, G., Chappell, S., Do, T., Lu, J. R., Matthews, K., Meyer, L., Stockton, A., Wizinowich, P. and Yelda, S. (2014), Detection of Galactic Center Source G2 at 3.8 μm during Periapse Passage, *ApJL*, **796**, L8, arXiv: 1410.1884.

Yuan, F. and Narayan, R. (2014), Hot Accretion Flows Around Black Holes, *ARA&A*, **52**, pp. 529–588, arXiv: 1401.0586.

Zajaček, M., Britzen, S., Eckart, A., Shahzamanian, B., Busch, G., Karas, V., Parsa, M., Peissker, F., Dovčiak, M., Subroweit, M., Dinnbier, F. and Zensus, J. A. (2017), Nature of the Galactic centre NIR-excess sources. I. What can we learn from the continuum observations of the DSO/G2 source?, *A&A*, **602**, A121, arXiv: 1704.03699.

Zajaček, M., Eckart, A., Karas, V., Kunneriath, D., Shahzamanian, B., Sabha, N., Mužić, K. and Valencia-S., M. (2016), Effect of an isotropic outflow from the Galactic Centre on the bow-shock evolution along the orbit, *MNRAS*, **455**, pp. 1257–1274, arXiv: 1510.02285.

Zhang, Q. and Zheng, X. (1997), The Role of Bow Shocks in Bipolar Molecular Outflows, *ApJ*, **474**, pp. 719–723.